EPiC Series in Engineering

Volume 3, 2018, Pages 1397–1405

HIC 2018. 13th International Conference on Hydroinformatics

Extracting High Resolution Snow Distribution Information with Inexpensive Autonomous Cameras

Pauline Millet[3] , Hendrik Huwald[2] and Steven V. Weijs[1*]

[1] UBC, Dept. Civil Engineering, 6250 Applied Science Ln, V6T 1Z4, Vancouver, BC, Canada

[2] School of Architecture, Civil and Environmental Engineering, Ecole Polytechnique Fédérale de Lausanne, EPFL, Lausanne, Switzerland

3 M.Sc. exchange student at 2 visiting 1; currently working at Makina Corpus, Toulouse, France

steven.weijs@civil.ubc.ca

Abstract

This study details a procedure to derive high resolution snow cover information using low-cost autonomous cameras. Images from time lapse photography of target areas are used to obtain temporally resolved binary snow-covered area information. Various image processing steps, such as distortion correction, alignment, projection using the Digital Elevation Model (DEM), and classification using clustering are described. Several innovations, such as matching the mountain silhouette with the DEM, and application of specific filters are described to make this terrestrial remote sensing method generally applicable to derive valuable snow information.

1 Introduction

In hydrology and snow science, the snow water equivalent (SWE), is a key variable representing the quantity of water contained in the snowpack. It is essential to model hydrological processes in mountainous regions where water is temporally stored in form of snow as this provides relevant information to various domains such as land and water management, agriculture, ecology and natural hazard prevention [1]. The spatial distribution of snow in mountains is difficult to estimate due to terrain complexity, unpredictable meteorological conditions or effects resulting from wind and radiation interaction with the terrain, leading to large spatial variability of SWE within a given catchment [2]. As a result, economically measuring snow cover evolution at spatial scales between the point and the satellite pixel has been elusive.

Time-lapse photography is an increasingly used technique for monitoring the environment. The technique has recently been implemented in various catchments for modelling the snow cover evolution to assess the effect of topography on snow spatial distribution [3,4]. Snow cover information can be combined with numerical snow cover models to get information on SWE.

Corripio [5] has developed a methodology for geo-referencing terrestrial photography for snow albedo estimation. Based on the camera location and orientation, a virtual view of the digital elevation model (DEM) grid can be projected on the picture of the studied terrain. The information in the photograph pixels are consequently directly associated locations on the map. Coupled with time-lapse photography, this approach has an important potential in monitoring applications by its easy implementation, its low cost of installation and the high spatial and temporal resolutions of the data provided over small-scale catchments.
The main purpose of this paper is to describe some practical hurdles and innovative solutions to overcome them in application of a procedure for snow cover extraction to a case study in the Swiss Alps. We describe several elements for an automated procedure for snow detection in the terrain that can use pictures from different sources at different locations. These elements form steps towards the applicability of a large-scale crowdsourced snow information collection. Recently, a few promising approaches in this direction have been launched and carried out, for instance the citizen observatory WeSenseIt[1] or the snow depth collection project SnowAlp[2] [6].

2 Study area and data used for the development

From 2008 to 2014, data was acquired at various locations in the Val Ferret catchment, Switzerland, to capture spatial variability of the environmental variables over a complex mountainous terrain. In addition to numerous meteorological stations of the project [7,8], three inexpensive cameras (Canon PowerShot A490 and A495) were converted into solar powered autonomous cameras and placed at two different locations to evaluate snow cover evolution by means of hourly photographs, from 2012 to 2014. In this study, as a proof of concept, pictures from two cameras with different orientation, mounted side by side near the summit of *La Dotse*, are analysed over the period May 15 to June 27, 2012.

3 Description of the methodology

To make time-lapse photography a valuable tool in the context of snow monitoring, it is needed to have an approach, which is applicable in any situation and also able to manage the possible changes of the camera position for time series processing. In this study, an automated processing of pictures has been designed for tracking snow evolution in the camera's viewshed. The procedure is composed of two steps, (a) pictures' alignment and (b) snow pixel extraction, and should handle a large number of acquired photographs, in a reasonable computational time. The method is presented below step by step.

3.1 Alignment of pictures

Due to wind effects on the cameras mounted on 2 meter poles with guy wires, or slight changes in the ground surface, the field of view is not constant over time. The first key aspect is then to stabilize the pictures for reliable time series analysis. This consists of rotating and translating pictures such that any physical point is always at the same place on the pictures. Since changes in the camera position are limited, influence on the variation of scale on large landscape pictures is small. Bad quality pictures are discarded to avoid misclassification at the snow extraction step. The following sections present the steps of image processing applied to the sequence of pictures to produce a suitable data set for further analysis.

[1] More information on the website: wesenseit.com.
[2] More information on the website: arpa.vda.it.

3.1.1 Distortion correction

Distortion is an optical aberration due to the lens of the camera. It results in an altered image of the reality, making rectilinear projection inapplicable. In the classification step in this study, correction is needed to ensure correct geo-referenced projection of the DEM on the picture. For this, the camera lens specifications were determined and images were corrected accordingly.

3.1.2 Image stabilization and picture removal

Time series images are repositioned relatively to each other's. From each picture, some local features, such as edges or corners, can be detected, and their properties and location extracted. For pictures of the same object, the extracted features should be similar, regardless of the camera position and orientation. This allows to compute feature point pairs between images to determine the transformation between two pictures as shown in Figure 1. The transformations are applied on the time series so that all the pictures are correctly aligned.

The same features can be useful to remove bad quality pictures: being usually more or less plain (snow on lens / clouds in valley), only a few features are detected on those pictures. Pictures not meeting a minimum number of detected features needed for further processing were removed.

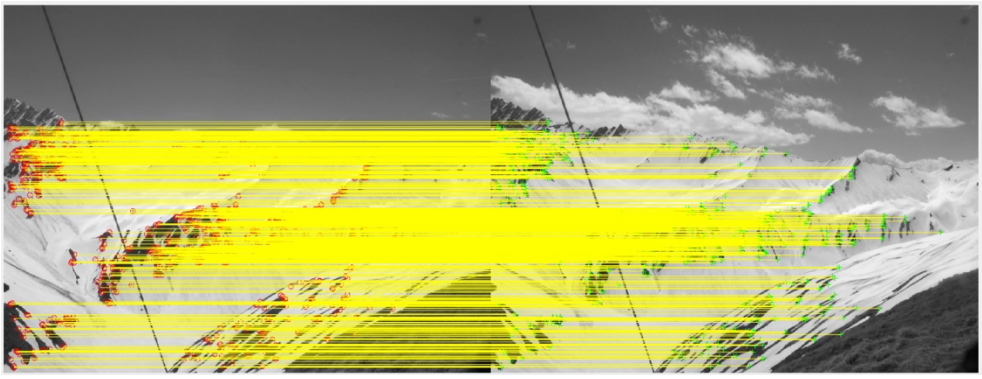

Figure 1. Two consecutive pictures with many matching features. The red and green markers design the features' locations while the yellow lines show the features' matches.

3.1.3 Silhouettes matching

The camera location and the ground control points provided by the user may not be accurate enough to allow for a simple projection of the DEM on the pictures in the next steps. We introduce here a method to increase precision and enable further automation of the procedure.

The algorithm finds the necessary transformation to fit the mountains' silhouette extracted from a clear photograph in the time series with the one extracted from the DEM virtual view (Figure 2 (a) and (b)). The latter is computed from the viewshed based on the camera location and the target point (the real world location corresponding to the centre of the picture), according to [5]. It depicts a 2D projection image of the terrain according to the DEM and the camera orientation. The fit between the two silhouettes is measured through the normalized 2D cross correlation of the pictures [9,10]. From the maximum correlation found, the transformation between the two silhouettes is applied on all the pictures of the time series (Figure 2 (c) and d)).

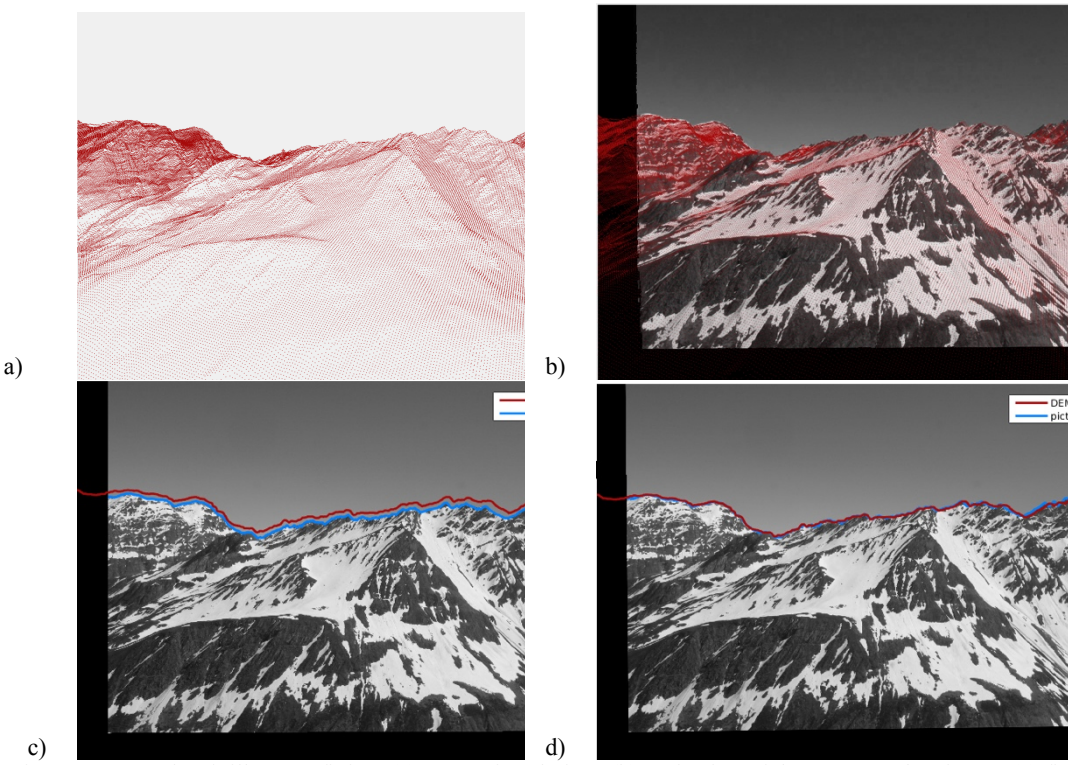

Figure 2. Example of silhouette fitting: (a) DEM virtual view, (b) projection of the DEM on the picture, (c) fit of DEM and silhouette, (d) fit after aligning DEM and picture. In this example, the correlation was 0.76 after a rotation of 0.5° and a translation of 6.5 pixels up and 0.5 pixels left.

3.2 Snow classification

An automated procedure requires robust and efficient snow detection in most situations. For the establishment of snow cover from terrestrial photographs [11], and [12] set a simple threshold on the blue channel but this technique implies to define a different one on each picture, in order to respond to changes in the weather and light conditions. A Normalized Difference Snow Index (NDSI) based on visible light (VIS) has been developed by [13] to bypass this issue. Nevertheless, a non-supervised method as the one suggested by [3] appears to be more appropriate. Because of the changing weather conditions, snow classification cannot be simply based on a defined colour threshold: snow may be a brilliant white surface during a sunny day but appears grey or has shade of blue under other light conditions. Even on a clear sky day, light conditions on a slope of a given exposition change over a day as a result of the trajectory of the sun in the sky. An automatic, non-supervised algorithm should to be able to deal with these variations during a day. However, the pixels representing snow are supposed to have similar colour properties within a single photography.

We proceed using the K-means algorithm [14], a non-supervised clustering approach, for snow classification, as it has already proven its efficiency for this purpose on terrestrial photographs [3,15]. The algorithm aims at forming n groups with comparable properties. The similarity between the object and the group is evaluated using the Euclidean distance between the object's value and the mean value of the group. For the snow detection, the objects are the picture's pixels, and the classification is realized on their associated values on the red, green and blue (RGB) bands. The desired output is two pixels groups representing the categories *snow* and *no-snow*. Due to the presence of hard shadows on the snow surface during some times of the day, or the appearance of greenish patches in summer, the number of groups created from the K-means algorithm is set to 4, and these

are labelled: *snow*, *shadowed snow*, *light rock/meadow*, *dark rock*. The four clusters are subsequently aggregated into two classes: *snow* and *no-snow*.

4 Results

4.1 Snow classification

Figure 3 presents snow classification results from our case study. A mask, computed from the mountains' silhouette, is applied on the picture to exclude the sky from influencing the clusters. Shadows from clouds are identified and labeled in the correct category (Figure 3 (b) and (f)), as well as the green meadow (Figure 3 (h)). The first two clusters (*snow* and *shadowed snow*) are then aggregated into a single one being *snow* and the two other ones into *no-snow*.

As one can notice by comparing Figure 3 (c) and (d), some misclassification may occur due to particular light conditions and long distance of objects from the camera. Rocks and snow in the shadow of the back mountain (left side of the picture) are almost identical in color and barely distinguishable. To reduce the error associated with shadow, it has been chosen, to pick only the photographs shot between 11 a.m. and 4 p.m., when the sun zenith angles are smallest during the day. The picture presented in Figure 3 (c), shot at 10 a.m., is then removed from the initial pictures set. Misclassification also exists in areas composed of really light grey rocks. On Figure 3 (e) and (f), the light cloud shadow on snow does not affect clustering but some small rocky regions are labelled as *shadowed snow*.

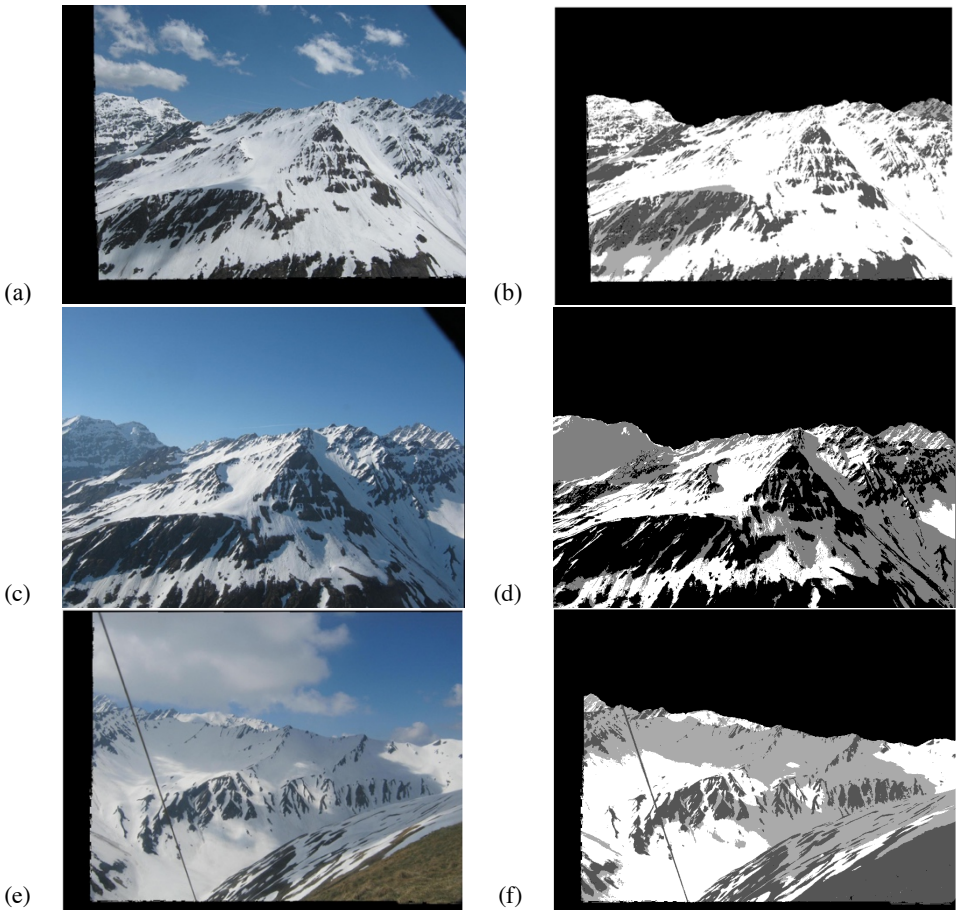

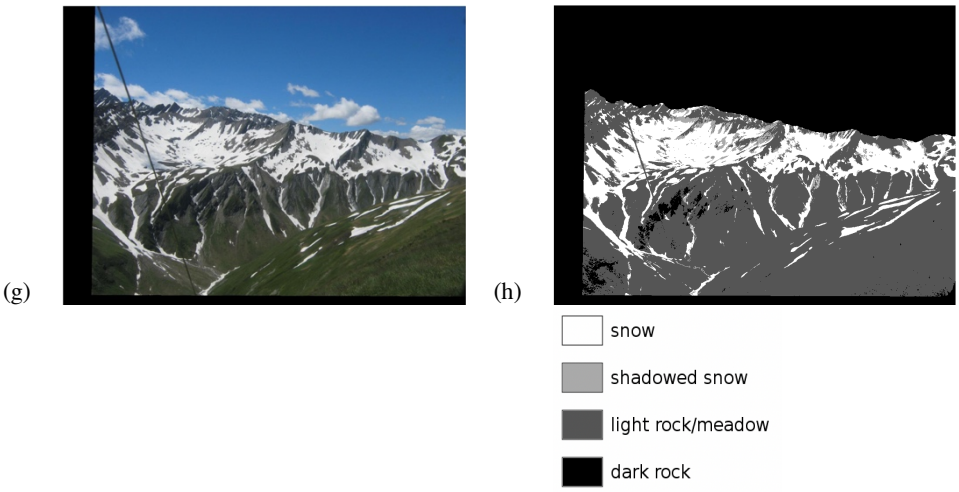

Figure 3. Snow classification by the K-means algorithm. Left: original pictures, right: classification results.

4.2 Snow cover and melt-out date maps

The snow classification result is associated with the DEM's cells through the virtual DEM view in order to obtain a map of the snow cover in the visible part of the catchment. From these observations, it is possible to produce maps of snow cover evolution over the catchment. Figure 4 (a) shows a map of the date of snow disappearance for the viewshed of the camera.

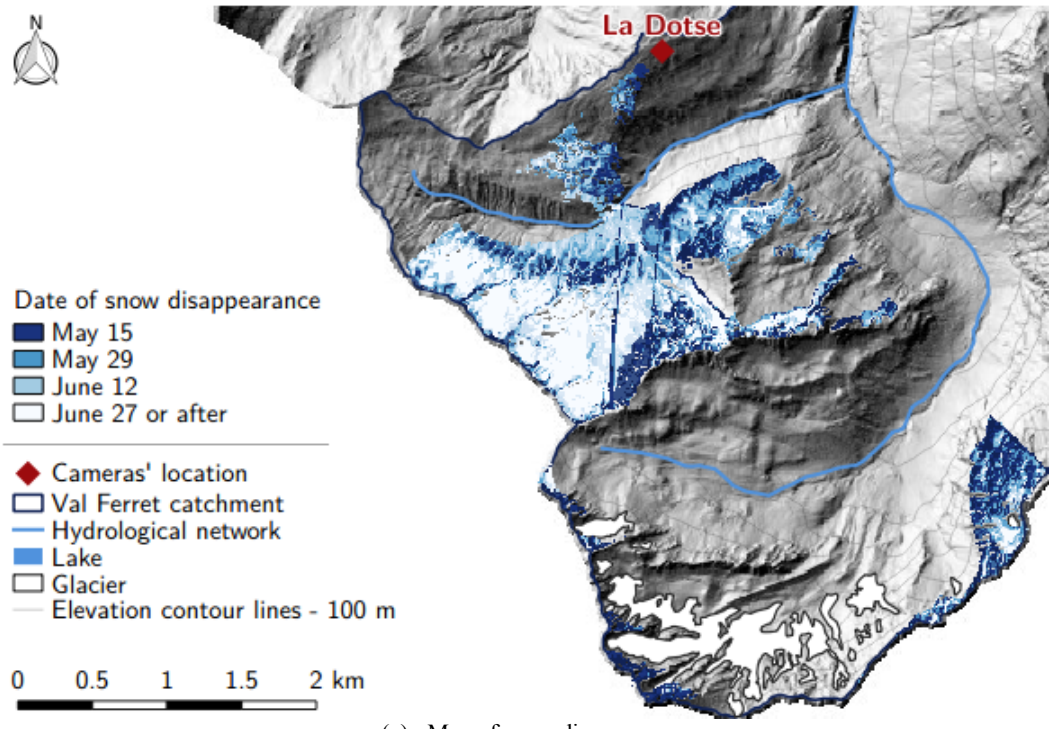

(a) Map of snow disappearance

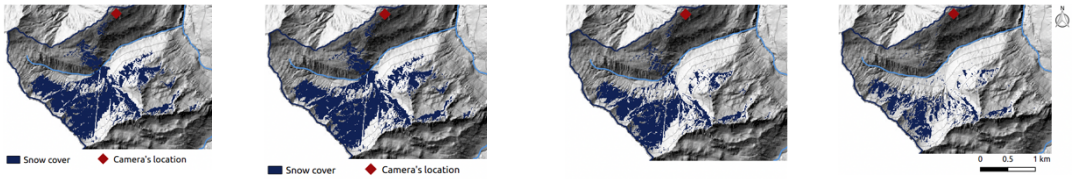

(b) 15 May (c) 01 June (d) 15 June (e) 27 June

Figure 4. Map of snow disappearance date and time series of snapshots over the melting period.

Figure 4, including the snapshots of the snow-covered area, can be reconstructed from a single -ascii file containing a map of the melt-out date. It should be noted, however, that in case accumulation events occur during the melt season, a melt-out date map would no longer contain all information, and a series of snapshots needs to be saved. The available data also allow for the computation of snow depletion curves, an example for the results obtained from the camera at the Dotse site is shown in Figure 5.

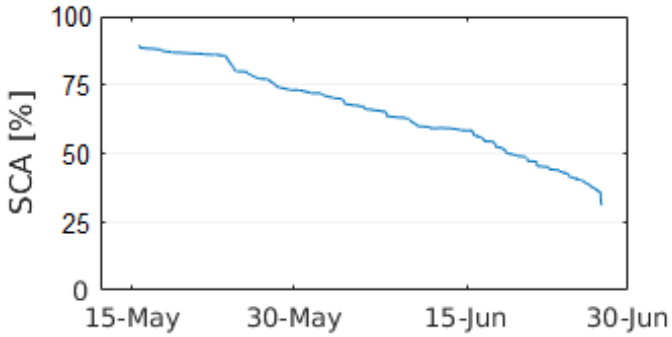

Figure 5. Snow cover depletion curve for the observed area.

5 Discussion

As visible in Figure 4, time-lapse photography of the catchment provides snow extent evolution at high spatio-temporal resolution. While the time component depends on the number of pictures retrieved after the alignment process, spatial resolution mainly depends on the DEM resolution. Regarding the computational time demand, the procedure took approximately 30 minutes on a regular PC to handle the initial 773 images from one of the two cameras and finally obtain the snow map Figure 4 (a). Employing this quantity of images may be excessive and using only one or two pictures per day may be sufficient and would reduce the computation time.

Although time-lapse photography offers high-resolution monitoring of a catchment, several sources of errors may lead to a wrong mapping. The accuracy of the picture decreases with distance since the pixels represent larger areas, resulting in a less precise snow detection in the remote areas than in the zones closer to the camera. Along the same idea, even if the match between the DEM and the picture silhouettes is rather good, a slight drift may exist. A tiny difference on the picture corresponds to an important distance in reality, leading to errors on the projected map. It is all the more important in mountainous regions: due to highly variable topography, snow accumulation may be very different between two close locations.

Apart from spatial issues, the snow detection step could misclassify pixels when bad quality images are not removed in the previous stage. Identifying elements, such as clouds, on the picture is challenging using visible range only. The high frequency of observations enables a cross check of the classification with pictures from the previous and next epochs.

The accuracy of the classification still needs to be assessed. Nonetheless, similar snow depletion curves were retrieved for the two studied time series, while the classification process is independent for the two locations, which is a promising sign regarding the robustness of the results.
To extract more information from the time-lapse photography, graduated poles should be deployed in the near range of the camera, as suggested by [4] to estimate the snow height evolution. Automatic reading of the graduated poles is also possible via image processing.

6 Conclusion

Time-lapse photography constitutes an interesting alternative to conventional terrestrial remote sensing techniques for the monitoring of a catchment. The proposed methodology is intended for hydrological applications, particularly given the low implementation requirements and the high resolution of the outputs. The resulting maps help studying snow distribution and its relationship with topographic factors. Image processing should be tested further with photographs originating from other sources, e.g. hikers, skiers or ski resort webcams. The silhouettes matching, as well as the geo-localisation from GPS data stored in cell phone pictures, would be key aspect for handling these pictures in the automated procedure. The algorithm could also be integrated in a snow monitoring system to update snow forecast in real time, according to the snow cover observations.
Follow-up work is focusing on combining the snow cover information with a snow physics model, with the aim of deriving information on snow depth and snow water equivalent by data assimilation of the binary snow cover information into the model results that ensure mass and energy balance.

7 References

[1] J.D. Lundquist, M.D. Dettinger, How snowpack heterogeneity affects diurnal streamflow timing, Water Resour. Res. 41 (2005).
[2] T. Brauchli, E. Trujillo, H. Huwald, M. Lehning, Influence of Slope-Scale Snowmelt on Catchment Response Simulated With the Alpine3D Model, Water Resour. Res. 53 (2017) 10723–10739. doi:10.1002/2017WR021278.
[3] R. Pimentel, J. Herrero, M.J. Polo, Terrestrial photography as an alternative to satellite images to study snow cover evolution at hillslope scale, in: SPIE Remote Sens., International Society for Optics and Photonics, 2012: p. 85310Y–85310Y.
[4] J. Parajka, P. Haas, R. Kirnbauer, J. Jansa, G. Blöschl, Potential of time-lapse photography of snow for hydrological purposes at the small catchment scale, Hydrol. Process. 26 (2012) 3327–3337.
[5] J.G. Corripio, Snow surface albedo estimation using terrestrial photography, Int. J. Remote Sens. 25 (2004) 5705–5729.
[6] M. Mazzoleni, M. Verlaan, L. Alfonso, M. Monego, D. Norbiato, M. Ferri, D.P. Solomatine, Can assimilation of crowdsourced data in hydrological modelling improve flood prediction?, Hydrol. Earth Syst. Sci. Katlenburg-Lindau. 21 (2017) 839–861. doi:http://dx.doi.org/10.5194/hess-21-839-2017.
[7] R. Mutzner, S.V. Weijs, P. Tarolli, M. Calaf, H.J. Oldroyd, M.B. Parlange, Controls on the diurnal streamflow cycles in two subbasins of an alpine headwater catchment, Water Resour. Res. 51 (2015) 3403–3418. doi:10.1002/2014WR016581.
[8] S. Simoni, S. Padoan, D.F. Nadeau, M. Diebold, A. Porporato, G. Barrenetxea, F. Ingelrest, M. Vetterli, M.B. Parlange, Hydrologic response of an alpine watershed: Application of a meteorological wireless sensor network to understand streamflow generation, Water Resour. Res. 47 (2011) W10524. doi:10.1029/2011WR010730.
[9] K. Briechle, U.D. Hanebeck, Template matching using fast normalized cross correlation, in: AerospaceDefense Sens. Simul. Controls, International Society for Optics and Photonics, 2001: pp. 95–102.

[10] D.-M. Tsai, C.-T. Lin, Fast normalized cross correlation for defect detection, Pattern Recognit. Lett. 24 (2003) 2625–2631.
[11] S. Schmidt, B. Weber, M. Winiger, Analyses of seasonal snow disappearance in an alpine valley from micro-to meso-scale (Loetschental, Switzerland), Hydrol. Process. 23 (2009) 1041–1051.
[12] J. Revuelto, T. Jonas, J.-I. López-Moreno, Backward snow depth reconstruction at high spatial resolution based on time-lapse photography, Hydrol. Process. (2016).
[13] J. Hinkler, S.B. Pedersen, M. Rasch, B.U. Hansen, Automatic snow cover monitoring at high temporal and spatial resolution, using images taken by a standard digital camera, Int. J. Remote Sens. 23 (2002) 4669–4682.
[14] J. MacQueen, others, Some methods for classification and analysis of multivariate observations, in: Proc. Fifth Berkeley Symp. Math. Stat. Probab., Oakland, CA, USA., 1967: pp. 281–297.
[15] M.J. Pérez-Palazón, R. Pimentel, J. Herrero, M.J. Polo, Analysis of snow spatial and temporary variability through the study of terrestrial photography in the Trevelez river valley, in: SPIE Remote Sens., International Society for Optics and Photonics, 2014: pp. 923918–923918.